Chapter 5. Kolsky Compression Bar Experiments on Ductile Materials

Ductile materials initially deform elastically and then plastically to large strains. The material stiffness is quite different in elasticity and plasticity. Experiment design may be focused on the response in either elasticity or plasticity, but mostly in the latter. This chapter describes the distinct characteristics of ductile materials, introduces a compound pulse shaper to maintain constant plastic strain rates. Examples are then given with the specimen materials being metals, a shape-memory alloy, an alumina particle-filled epoxy, and a lead-free solder.

5.1 Issues in Kolsky-Bar Experiments on Ductile Materials

Traditionally, the Kolsky bar has been widely used to characterize the high-rate flow behavior of ductile metals. When the specimen enters plastic deformation, it can deform to large strains at high strain rates. However, it has been recognized in the past decades that the Kolsky bar cannot obtain valid elastic response of ductile materials (Gray 2000). For example, the rate-independent moduli of elasticity of alloys measured from Kolsky-bar experiments are usually only 30% to 50% of the values obtained from quasi-static experiments. The reason for the erroneous elasticity measurement is due to the inaccurate measurement in specimen deformation. In Kolsky-bar experiments, it is typically more challenging to measure the specimen deformation than the stress, particularly when the specimen is subjected to small deformation. Many traditional alloys have been recognized that their elastic moduli are independent of strain rate. The inaccurate measurement in elastic response may not be serious for these materials. However, more attention should be paid to the ductile materials that exhibit significant strain-rate sensitivities even in elastic response, for example, shape memory alloys. Moreover, the elastic response is required to be accurately measured for those materials whose responses are not known yet.

There are three sources that may lead to inaccurate measurements in specimen deformation. The first one is wave dispersion. As discussed in Chapter 2.1, the stress wave dispersion results in different signals at the specimen/bar end interfaces from those recorded by the strain gages in the middle of the bars. Without dispersion correction, the specimen strain

W.W. Chen and B. Song, *Split Hopkinson (Kolsky) Bar: Design, Testing and Applications*, Mechanical Engineering Series, DOI 10.1007/978-1-4419-7982-7_5,

directly calculated with the signals from the strain gages deviates from the actual strain to which the specimen is subjected. The deviation is so significant, in comparison to the elastic strain in the specimen, that the measured modulus is erroneous, usually smaller, even though the stress measurement is accurate (Zhao and Gary 1996). Correcting the stress wave dispersion with either numerical method or physical pulse shaper can improve the accuracy of the elastic response for ductile materials. However, wave dispersion correction alone is not sufficient to accurately determine the elastic moduli. At the beginning stages of the high-rate loading, more complications are encountered in the accurate determination of strain history.

In a Kolsky-bar experiment, it takes only a few microseconds for the ductile specimen to yield due to its small yield strain. The stress may not be in equilibrium yet within such a short duration, particularly when the initial rate of loading is high. The non-equilibrated stress state in the specimen results in non-uniform deformation through its thickness direction. Taking an average in both stress and strain over the specimen length, as expressed by (1.7) and (1.15), may yield smoother results. However, this is artificial and does not reflect the actual loading and deformation states in the specimen. In order to achieve the specimen stress equilibrium when the strain is still low, the initial rate of loading must be low. A trade off of this low rate of initial loading is to sacrifice the strain rate. For example, the strain rate in elasticity is below 100 s^{-1} to obtain accurate elastic response for elastic-plastic alloys (Chen et al. 2003).

As presented in Chapter 2.5, pulse shaping makes Kolsky-bar experiments more controllable for not only stress equilibrium but also constant strain-rate deformation in specimen. The constant strain-rate deformation is desired for the specimen even under elastic deformation, particularly when the specimen material is highly strain-rate sensitive, such as shape memory alloys. Similar to the brittle material characterization discussed in Chapter 3 where there is a limit in achievable constant strain rate, the ductile specimen may yield before the strain rate reaches a constant because it takes time for the specimen to accelerate from rest to the high strain rate. Strain is accumulated in the specimen during this acceleration process. This also limits the maximum achievable elastic strain rate in Kolsky-bar experiments on ductile materials. When the specimen deforms beyond its elastic limit, its stiffness decreases drastically. This results in a sudden increase in strain rate. When ductile materials are investigated at high rates, the “strain rate” is usually referred to the later plastic strain rate, which is typically 1-2 orders higher in amplitude than elastic strain rate achieved in the same experiment.

Another source for erroneous measurement in elastic response is the possible indentation to the bar ends by a stiff specimen (Safa and Gary

2009). This indentation results in severe non-planar stress waves. Furthermore, the particle velocity at the incident bar/specimen interface is higher; whereas, the particle velocity at the specimen/transmission bar is lower, than those the specimen actually experiences. Consequently, the calculated strain rate and strain in the specimen becomes higher, which leads to lower modulus of elasticity. In order to prevent such an indentation when characterizing high-strength ductile materials, stiff platens are needed, as discussed in Chapter 3.

Before yielding, most ductile materials behave in the same manner as brittle materials with high stiffness. The Kolsky bar method for brittle material characterization is applicable in the characterization of the elastic response of ductile materials. After yielding, the tangential modulus in the stress-strain curves for ductile materials drops sharply in plastic deformation. The linear ramp pulse for brittle materials is not applicable any longer. Instead, the profile of the incident pulse needs to be further modified according to the work hardening response of the ductile material under investigation. If the material possesses significant work hardening response, the traditional flat-top loading pulse is typically unable to maintain a constant strain rate at large strains. A typical set of oscilloscope records from conventional Kolsky-bar experiment on a work hardening ductile material are shown in Fig. 5.1 (Chen et al. 2003). The incident pulse needs to increase with time to maintain a constant engineering strain rate in the plastically deforming specimen. In addition to the modification to the shape of the incident pulse, the amplitude of the incident pulse needs to be sufficiently high to compress the ductile specimen at high strain rates. This brings another challenge in pulse-shaping design where a soft material such as annealed copper is usually employed as the pulse shaper.

If, in addition to the loading stage, the unloading process needs to be controlled, the pulse in the unloading part must be shaped accordingly. A typical example of this class of experiments is the characterization of the dynamic stress-strain loops of shape-memory alloys. As can be imagined, these experiments are more challenging to perform.

Since ductile materials are capable of large deformation, the specimen will significantly expand along lateral directions when it is subjected to large deformation under axial compression. At large deformation, the interfacial friction at the bar end/specimen interfaces may restrict the lateral expansion of the specimen. In this case, the specimen under large deformation is in a shape of barrel, revealing three-dimensional stress state at the specimen ends. Therefore, the interfacial friction should be minimized in Kolsky-bar experiments on ductile materials to large deformation.

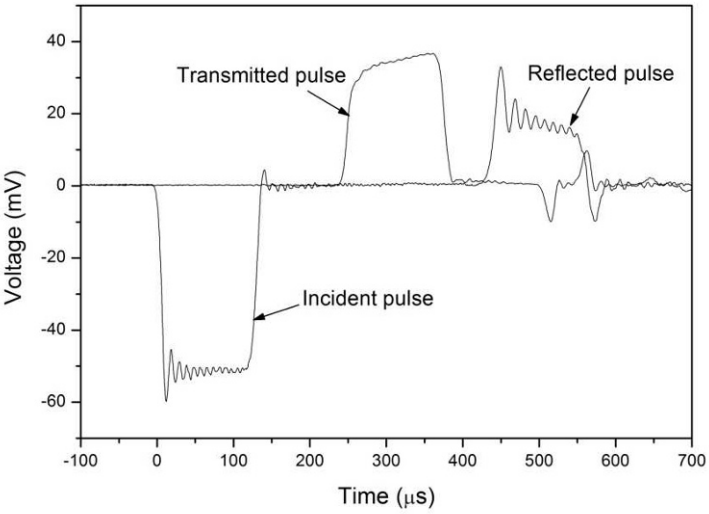

Figure 5.1 Typical oscilloscope records in a conventional Kolsky bar experiment on a work-hardening material *(Reproduced from Chen et al. (2003) with permission)*

5.2 Pulse Shaping

In order to achieve constant strain rates in Kolsky-bar experiments on ductile materials, the incident pulse should have a profile similar to the transmitted pulse which is usually a representative of stress response of the specimen material. Trial experiments are needed to provide approximate information of such a stress response, giving a starting point in regard to the profile of the incident pulse needed for facilitating constant strain rate. For the ductile materials with work hardening behavior, the incident pulse is typically of similar work hardening profile but with a higher amplitude. As mentioned in the previous section, the specimen is desired to be stress equilibrated as soon as possible to obtain valid elastic response of the specimen material. The initial rate of loading in the incident pulse should be low. Therefore, the incident pulse needs to have a

profile as the one illustrated in Fig. 5.2 for characterizing most work hardening ductile materials.

A single annealed copper disk is not sufficient to serve as the pulse shaper to produce a high-amplitude incident pulse as illustrated in Fig. 5.2 due to the low yield strength of copper. The dual pulse shaping technique as shown in Fig. 2.16 is needed for ductile material characterization. The dual pulse shaping generally consists of a soft pulse shaper, such as copper, stacked on a second pulse shaper made of a hard ductile material such as steel. The striker impacts on the copper disk first. Due to its low strength and high ductility, the copper disk is extensively compressed, producing a nearly linear but low-amplitude pulse. The rate of loading is relatively low at this stage. This produces the early portion in the incident pulse. When the copper disk is subjected to continuing compression, it eventually becomes extremely thin and nearly incompressible. The second ductile pulse shaper, e.g., steel, starts to play its role in shaping the incident pulse. Due to its typical elastic-plastic characteristic, the pulse transmitted through the second pulse shaper possesses a similar linear elasticity followed by a work hardening response. The amplitude depends on the flow strength and dimensions of the second pulse shaper, as well as the striking speed. In other words, the second pulse shaper dominates the incident pulse; whereas, the copper pulse shaper only lowers the rate of loading for the initial portion in the incident pulse. Combination of the material and dimensions of the first pulse shaper, as well as striking speed, is used to determine the initial loading rate of the incident pulse so that the specimen can be in stress equilibrium quickly. The material for the second pulse shaper is selected to have similar plastic flow behavior as the specimen material under investigation so that constant strain rate is achievable. When unloading stress-strain response of some ductile materials is investigated, reverse pulse shaping technique in association with momentum trap described in Fig. 2.22 should be employed to unload the specimen at the same constant strain rate as that in the loading portion. The reverse pulse shaping design depends on the unloading response of the specimen material, which is case by case.

It is noted that above strain rate refers to engineering strain rate. In some experiments, constant true strain rates, instead of constant engineering strain rates, are desired. Facilitating constant true strain rates is much more challenging in ductile material characterization. True strain (ε_T) can be calculated from engineering strain (ε_E) assuming the symbol takes positive in compression,

$$\varepsilon_T = -\ln(1-\varepsilon_E) \tag{5.1}$$

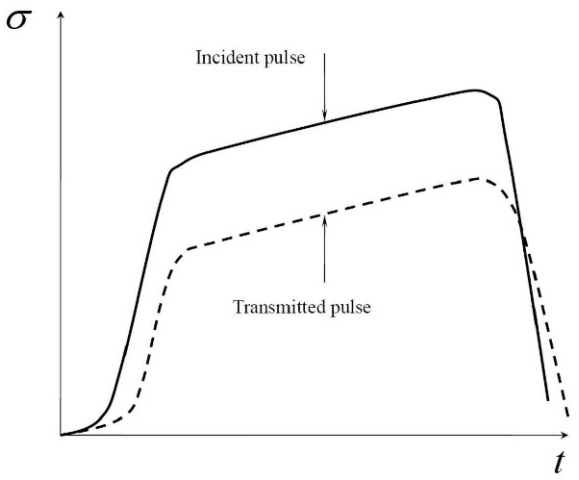

Figure 5.2 Illustration of pulse shaping design for ductile materials

Differentiating (5.1) with respect to time yields true strain rate

$$\varepsilon_T = \frac{\varepsilon_E}{1-\varepsilon_E} \tag{5.2}$$

Equation (5.2) can be rewritten as the following differential equation in terms of engineering strain,

$$\varepsilon_E + C\varepsilon_E = C \tag{5.3}$$

where $C = \varepsilon_T$ is a constant. Considering the initial condition,

$$\varepsilon_E\big|_{t=0} = 0 \tag{5.4}$$

Equation (5.3) has the solution,

$$\varepsilon = 1 - e^{-Ct} \tag{5.5}$$

or

$$\varepsilon_E = C \cdot e^{-Ct} \tag{5.6}$$

Since the reflected pulse represents engineering strain rate under stress equilibrium in a Kolsky-bar experiment, Equation (5.6) indicates that the reflected pulse should be in the form of exponential attenuation, as illustrated in Fig. 5.3, to facilitate constant true strain rate in specimen. Therefore, the pulse shaper should be carefully design to properly modify the incident pulse so that the reflected pulse schematically illustrated in Fig. 5.3 is produced. One approach is to use a tapered striker (Casem 2010).

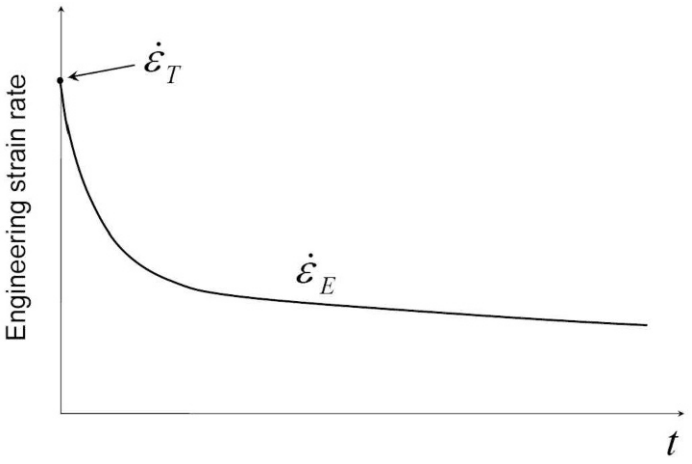

Figure 5.3 Engineering strain-rate history for constant true strain rate

5.3 Experiment Design for Ductile Materials

The experiment design for characterizing ductile materials depends on the specimen response, the desired testing conditions, and the strain range of interest. If the specimen material does not work-harden significantly and the main interest is to determine the dynamic flow stress as a function of plastic strain rate, conventional Kolsky bar experiments are very close to achieve the desired testing conditions on the specimen (constant plastic strain rate under dynamic equilibrated stress). The only undesired characteristic in the wave form is wave dispersion. With the knowledge of pulse shaping, a thin and small disk of a soft ductile material placed on the impact end of the incident bar can effectively minimize the wave dispersion. The specimen is then subjected to a well defined loading history. Changing the striking velocity will vary the strain rate in the specimen; whereas, changing the striker length varies the maximum strain in the specimen with a given thickness. It should be reminded that, in such experiments, the specimen is still in stress equilibrium process when the strains are small, the data at small strains may not be reliable. However, if the pulse shaper is properly designed so that stress equilibrium is achieved in the specimen at very early stages of loading, the elastic and early yielding response for the ductile specimen can be obtained accurately.

If the interest is on elastic and early plastic deformations, the response of the specimen is similar to that of a brittle material. Consequently, the pulse shaper design should be similar to the design for brittle materials. For those materials possessing strain-rate sensitivity in elasticity, the strain during initial strain acceleration should be small such that the most portion in elastic response and the following early plastic behavior are determined under valid conditions. As pointed out in Chapter 2.7, there exists a limit for achievable strain rate to determine the valid elastic response of the specimen material. It is noted that, if the elastic response of the specimen material is not sensitive to strain rate, such as most alloys, the initial strain acceleration does not affect the measurement of elastic response as long as the stress equilibrium is achieved. However, it is desirable that the strain rate reaches a constant before the specimen yields.

If the material has significant work hardening, dual pulse shaping is needed to facilitate constant strain rate and stress equilibrium. In the following section, we will present examples illustrating this case.

Most ductile materials can yield locally and are thus not very sensitive to stress concentrations. The hard platens and universal joints used in the experiments on brittle materials are typically not needed in the experiments, particularly when the ductile materials under investigation are more compliant than the bar material. However, when characterizing the ductile materials with high stiffness and strength, the platens are needed to obtain high-quality results and to protect the bar ends from indentation.

By contrast, some ductile materials, e.g., lead, may yield at low stress. The design of experiments for characterizing such materials is similar to that for soft materials. We will give an example of solder characterization in the last section of this Chapter.

5.3.1 Metals

We now take an example of characterizing the compressive response of 4340 steel alloy hardened to R_c45. The striker, incident, and transmission bars were 19.05-mm diameter C350 maraging steel. The incident and transmission bars had lengths of 3050 and 1525 mm, respectively, and the bar strain gages were located at 1670 mm from the impact end of the incident bar and at 245 mm from the specimen/bar interface on the transmission bar. The 4340 R_c45 specimen had a diameter of 6.35 mm and, to achieve a higher strain rate, a length of 3.11 mm.

A dual pulse shaping presented in Chapter 2.5 was employed. The dual pulse shaper consists of an annealed C11000 copper stacked on a 4340 R_c30 steel. Figure 5.4 shows the incident, reflected, and transmitted signals from such a dual-pulse-shaped experiment (Song et al. 2007a). The copper disk is 2.5 mm in diameter and 1.8 mm in thickness while the steel disk is 10.4 mm in diameter and 11.4 mm in thickness. The striker velocity was 29.95 m/s.

As seen in Fig. 5.4, the dual pulse shaping technique produced an incident pulse which has similar work hardening profile to the transmitted pulse. This is mainly contributed by the hard steel pulse shaper for the purpose of facilitating constant strain rate. A long toe region at the early stage of the incident pulse is also observed, which is the result of employing the soft anneal copper shaper. The initial slow rise in the incident pulse helps the specimen to achieve stress equilibrium quickly. In order to facilitate different strain rates, the striking velocity should vary, together with the dimensions of the copper and steel pulse shapers.

Figure 5.5 shows the incident pulses for different strain-rate characterization. The three incident pulses have similar profiles but different amplitudes, facilitating three different constant strain rates. Figure 5.6 shows the corresponding strain-rate histories. The strain rates obtained in the three experiments are nearly constants with different values, as observed in Fig. 5.6. The oscillations on the reflected pulses likely come from the high hardness of the specimen material. The strain rates can be calculated from averaging the oscillations in the strain-rate histories or the slope of its time integration (strain history).

Take an example of 1700 s^{-1} shown in Fig. 5.4, an average strain rate during the plastic flow strain rate of 1700 s^{-1} was measured from the slope of the strain-time curve over a time interval of 80 μs to 180 μs, as shown in Fig. 5.7 (Song et al. 2007a). At about 180 μs, the incident signal decays and the specimen begins to unload elastically. The stress comparison at both ends of the specimen is shown in Fig. 5.8 (Song et al. 2007a). The stress at the front end of the specimen is calculated using the difference in the incident and reflected strains (1.8), and the stress at the back end is calculated using the measured transmitted strain (1.9). The interface stresses are in reasonably good agreement, which implies that the specimen is nearly in dynamic stress equilibrium.

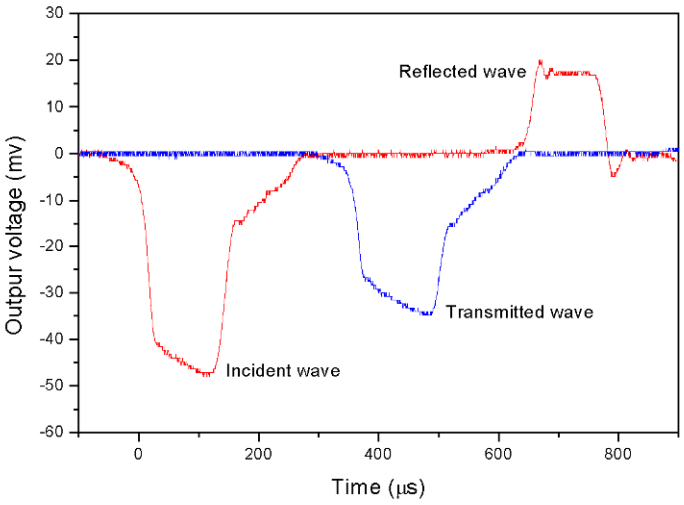

Figure 5.4 Experimental records of an experiment on 4340 steel
(Reproduced from Song et al. (2007a) with permission)

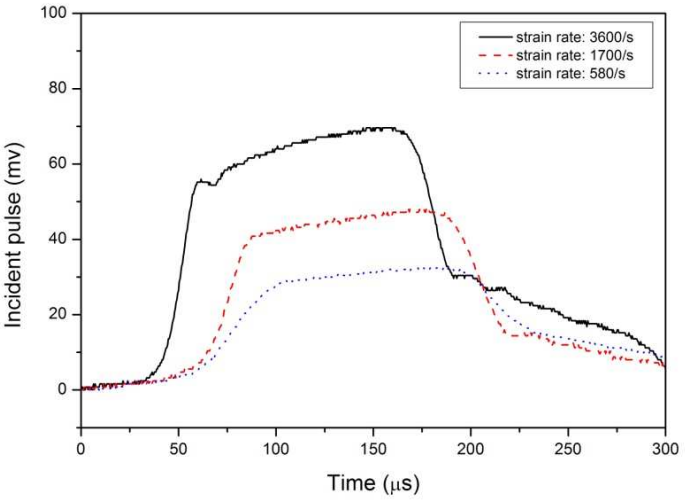

Figure 5.5 Pulse shaped incident pulses at various strain rates

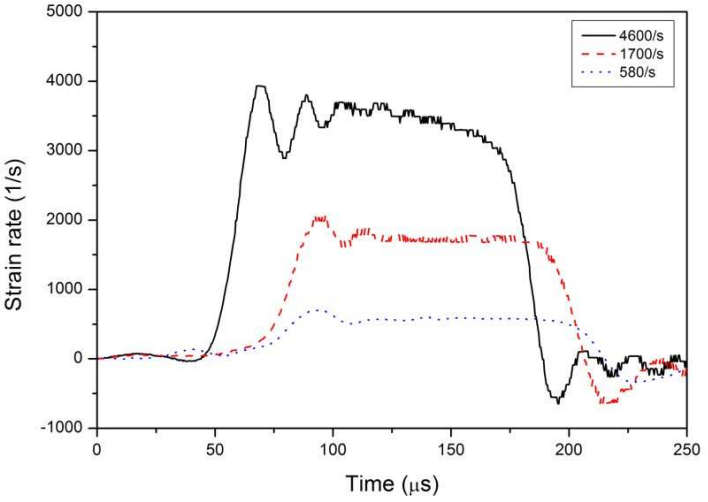

Figure 5.6 Strain rate histories

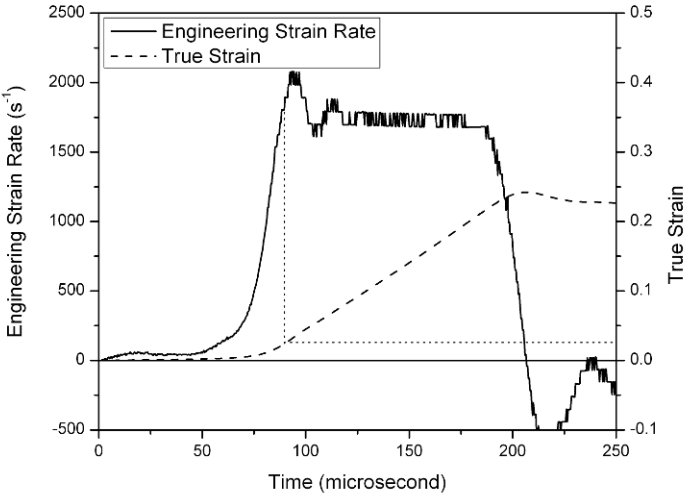

Figure 5.7 Time histories of strain rate and strain in the specimen
(Reproduced from Song et al. (2007a) with permission)

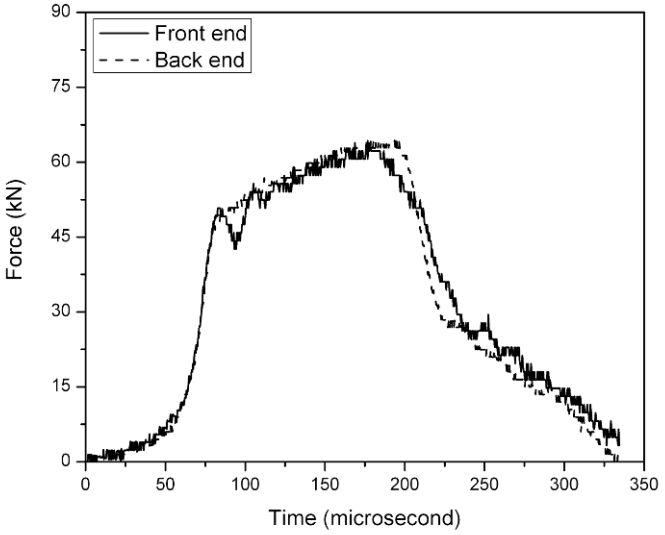

Figure 5.8 Comparison of stress histories at both ends of the specimen
(Reproduced from Song et al. (2007a) with permission)

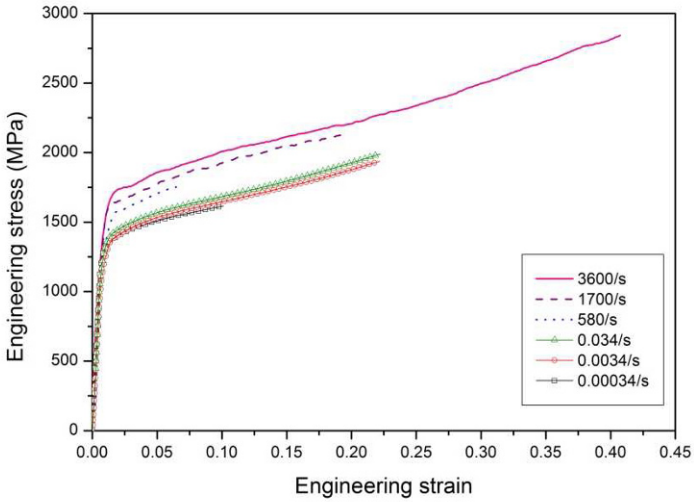

Figure 5.9 Engineering stress-strain curves of 4340 R_c45 steel
(Reproduced from Song et al. (2007a) with permission)

Figure 5.9 shows engineering compressive stress-strain curves of 4340 R_c43 steel at quasi-static and dynamic strain rates (Song et al. 2007a). The material exhibits linear elasticity followed by work hardening behavior with significant strain-rate effect. However, when the specimen is subjected to large deformation, engineering measurement may lack of interpretation of actual material response. Assuming the material is incompressible, the corresponding true stress-strain curves are shown in Fig. 5.10 (Song et al. 2007a). The true stress-strain curves show nearly perfect flow behavior. Strain-rate effect is still significant. At high strain rates, the strain accumulated within the strain acceleration stage may be over the yield strain. This results in relatively lower flow stress before the strain rate achieves the constant, as circled in Fig. 5.10. In order to determine the actual flow stress at the early stage, an analytical model was used to indirectly approach the early flow stress including the yield strength (Song et al. 2007a).

As shown in Fig. 5.10, the true stress-strain curves do not exhibit significant work hardening behavior. Instead, the stress softening is observed at high strain rates. This is due to the adiabatic temperature rise in the specimen during dynamic loading. A miniature thermocouple was

employed to measure the temperature rise in the specimen subjected to high-rate loading. The temperature rise histories in the specimens subjected to two different strain-rate loadings (1700 and 3600 s^{-1}) are shown in Fig. 5.11. The temperature rise softened the specimen, off-setting the work hardening. As an example, the true stress even becomes decreasing at high strain rates due to the significant temperature rise at large strains, as shown in Fig. 5.10.

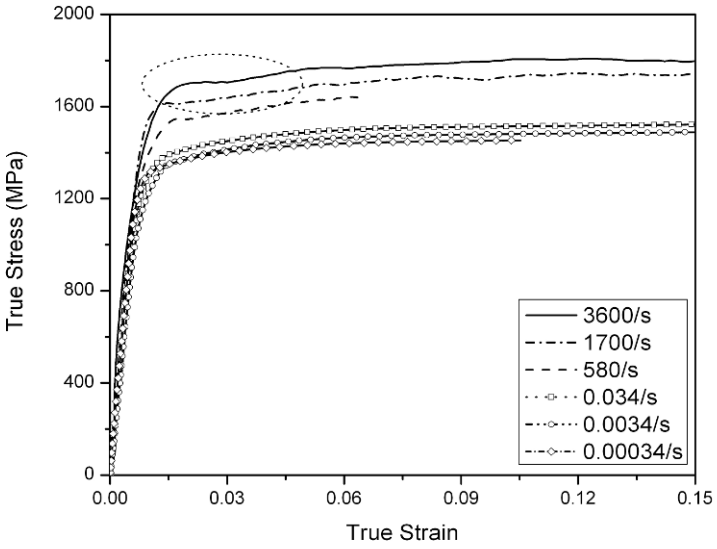

Figure 5.10 True stress-strain curves of 4340 R_c45 steel
(Reproduced from Song et al. (2007a) with permission)

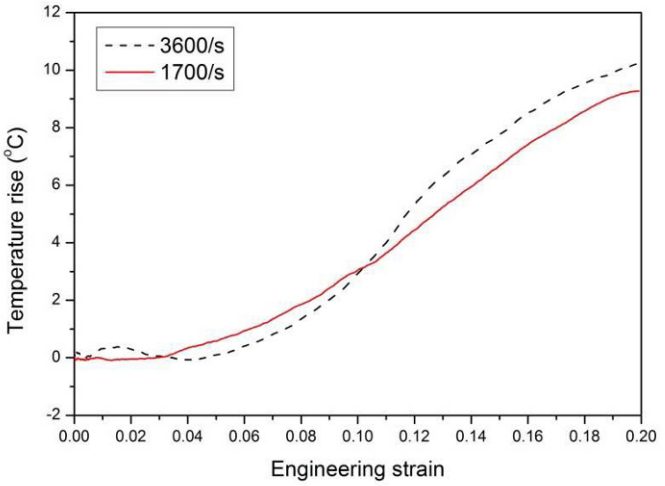

Figure 5.11 Temperature rise in the specimens at two different strain rates

When the specimen is subjected to high-rate loading, part of the produced plastic work at large deformation converts into heat in the specimen, resulting in temperature rise within the short loading duration. The fraction of the plastic work converted into heat can be estimated with the following equation (Hodowany et al. 2000),

$$\beta = \frac{\rho_s c_s \theta}{\sigma_T \varepsilon_{T,p}} \tag{5.7}$$

where β is the fraction of plastic work converted into heat; c_s is the specific heat of specimen material; θ is temperature-rise rate; and $\varepsilon_{T,p}$ refers to true plastic strain rate that can be calculated from engineering strain rate and strain with (5.2). Considering the specimen material is incompressible, the true stress (σ_T) in (5.7) can be calculated from engineering stress,

$$\sigma_T = (1 - \varepsilon_E)\sigma_E \tag{5.8}$$

The symbol for both stress and strain takes positive in compression here. Take an example, the values of parameters in (5.7) are listed in Table 5.1. The value of β is calculated as 0.76 with (5.7), indicating 76% of plastic work was converted into heat during the loading at the average true plastic strain rate of 1840 s^{-1}.

Table 5.1 Values taken for the parameters in (5.7)

Parameter	Value
ρ_s	7850 kg/m^3
c_s	477 J/kgK
θ	6.18×105 K/s
σ_T	1660 MPa
$\varepsilon_{T,p}$	1840 s^{-1}

With the use of dual pulse shaping technique, valid measurements of elastic and early plastic behavior can be obtained. We will give more examples showing the dual pulse shaping technique for ductile material characterization.

We now present the experiments on 1046 hot-rolled steel and 6061-T6 aluminum. Both steel and aluminum specimens had a common geometry with a length of 4.41 mm and a diameter of 8.88 mm. The dual pulse shaper consists of a half-hardened 1046 mild steel disk and an annealed *C*-11000 copper disk. The steel end of the dual pulse shaper is attached to the incident bar and the striker impacts the copper end.

Figure 5.12 shows the incident, reflected, and transmitted signals recorded from a typical experiment on the 1046 steel (Chen et al. 2003). With pulse shaping, the incident pulse was modified to produce a re-

flected signal with a nearly flat top that indicates a constant strain-rate history in the specimen. Furthermore, there is a small amplitude precursor ahead of the main reflected signal. Detailed data reduction reveals that this corresponds to the elastic deformation; whereas, the main reflected signal corresponds to the dynamic plastic flow in the specimen. During the elastic deformation, the specimen is stiff and deforms at a much lower strain rate. The details of this initial plateau in the reflected signal corresponding to the elastic deformation in the specimen are shown in Fig. 5.13 (Chen et al. 2003).

When the stress exceeds the dynamic yield strength, the stiffness of the specimen decreases significantly due to plastic flow, and this causes a much higher strain rate in the specimen. We note that the dynamic yield point is located at the transition between elastic and plastic strain response regions and the exact strain rate at dynamic yielding is actually not well defined. Figure 5.14 shows the dynamic compressive stress-strain curves from the experiments with and without pulse shaping at a close strain rate. The comparison shows that the difference in the elastic response is significant. The two curves start to merge after about 4% of strain.

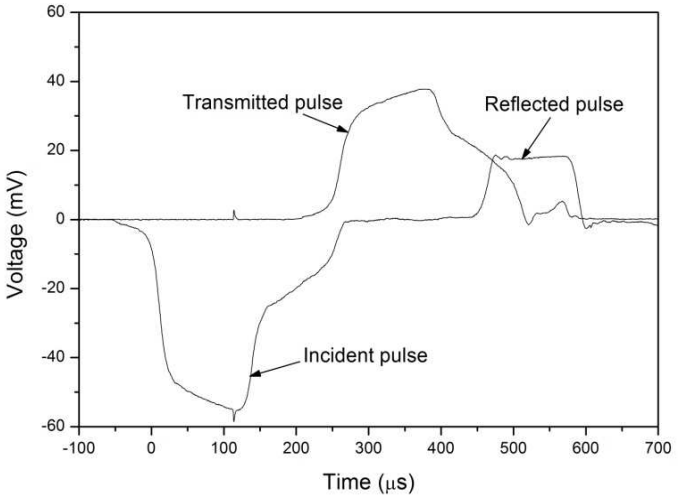

Figure 5.12 Oscilloscope records in a Kolsky bar experiment on 1046 steel
(Reproduced from Chen et al. (2003) with permission)

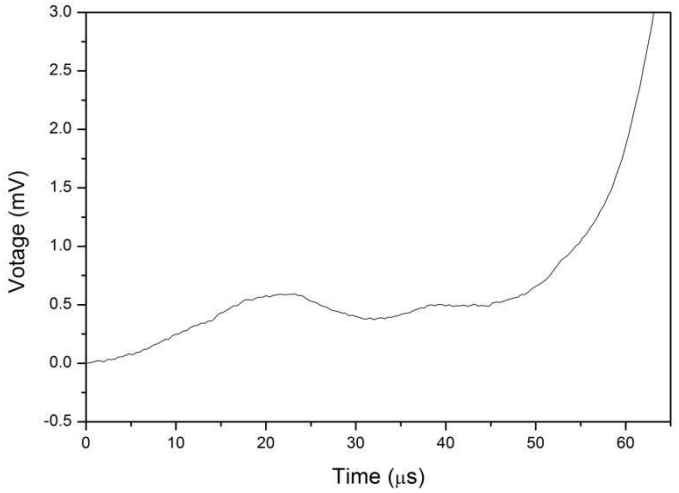

Figure 5.13 Reflected signal corresponding to elastic deformation
(Reproduced from Chen et al. (2003) with permission)

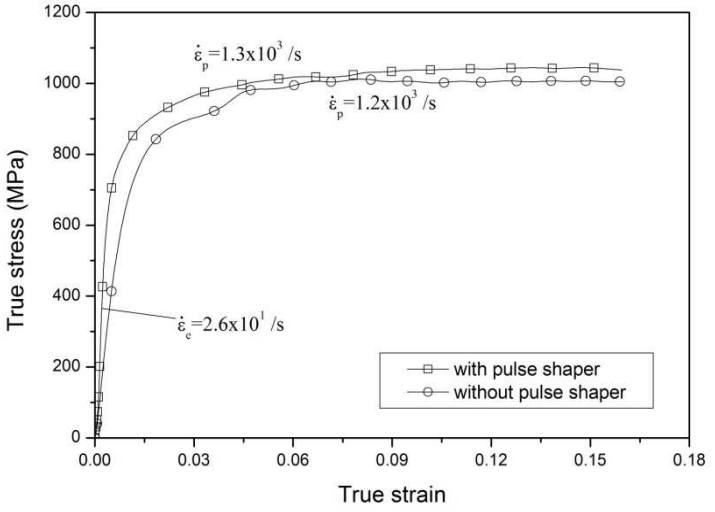

Figure 5.14 Dynamic stress-strain curves of 1046 steel from experiments with and without pulse shaping
(Reproduced from Chen et al. (2003) with permission)

Figure 5.15 shows oscilloscope records for 6061-T6 aluminum (Song et al. 2002), the characteristic of which is similar to the 1046 steel shown in Fig. 5.12. The initial portion with small amplitude in the reflected pulse is also observed, indicating the aluminum specimen deforms at a much lower strain rate in elasticity than that in plasticity. Figure 5.16 shows axial force versus time at the front end and the back of the specimen (Song et al. 2002). The nearly overlapping force histories in Fig. 5.16 indicate that the stress in the specimen is equilibrated very early in the experiment. The dynamic stress-strain curve reduced from this experiment is shown in Fig. 5.17 (Song et al. 2002). The Young's modulus from the stress-strain curve is approximately 70 GPa as determined from the early portion of the reflected and the transmitted signals shown in Fig. 5.15.

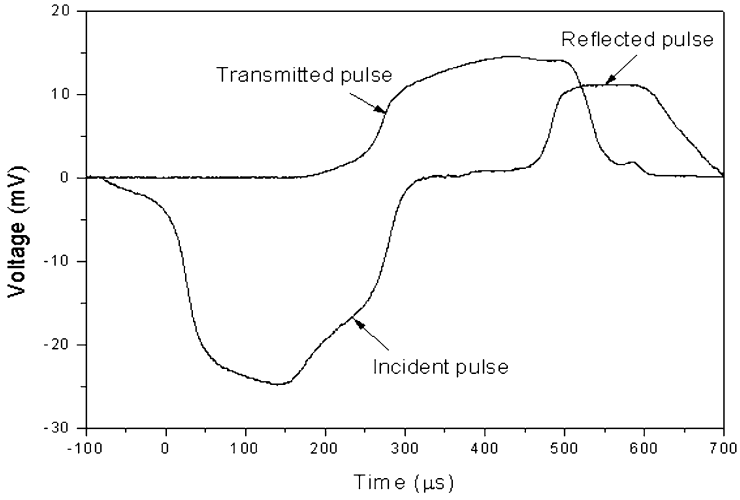

Figure 5.15 Oscilloscope records for 6061-T6 aluminum
(Reproduced from Song et al. (2002) with permission)

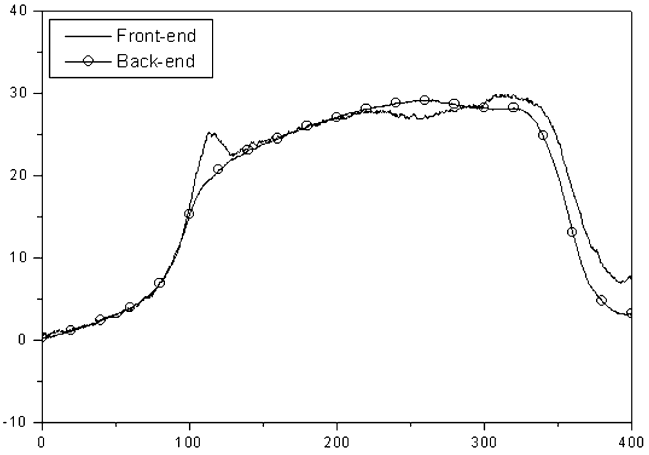

Figure 5.16 Comparison of force histories at both ends of the specimen
(Reproduced from Song et al. (2002) with permission)

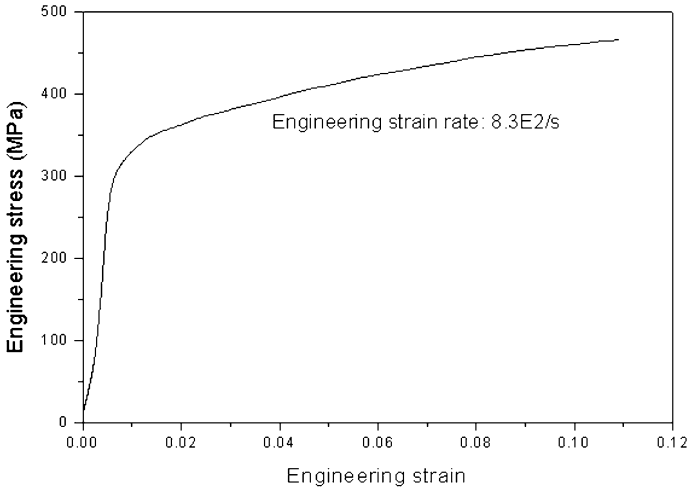

Figure 5.17 Dynamic stress-strain curve of 6061-T6 aluminum
(Reproduced from Song et al. (2002) with permission)

While conducting the experiments, it was noticed that the bar alignment and the specimen geometry, in particular the parallelism of the end faces, are very important in order to obtain accurate elastic behavior of the specimen material. The amplitude of the elastic precursor, from which the specimen elastic strain is integrated, is sensitive to the misalignment of the bars, the non-parallelism of the specimen ends, the flatness of the bar and the specimen end faces, and the initial contacting conditions between the specimen and the bars. These experiments demonstrate that, with proper pulse shaping, the data at small strains are not necessary invalid. In fact, the modulus of elasticity can be recovered. It is also noticed that, even with pulse shaping, not the entire elastic portion of the stress-strain curve was obtained under well-defined testing conditions. The specimen deformation accelerates from zero to a desired level. Strain is accumulated during this acceleration process. Therefore, the initial portion of the stress-strain curve is obtained during this acceleration process. However, this will not affect the elastic response for most metallic materials which are not rate dependent in elastic response.

5.3.2 Shape Memory Alloy

The stress-strain behavior of a shape memory alloy has distinct loading and unloading responses. Instead of a conventional stress-strain curve for most metals, a stress-strain loop that includes both loading and unloading portions must be characterized at a common constant strain rate. In this example, we present the design of a set of such experiments where both the loading and unloading portions of the pulses are controlled by pulse shaping, which is similar to the characterization of PMMA in Chapter 4.5.1. A reverse pulse-shaping technique described in Chapter 2.6 was used to generate an unloading profile to ensure the same constant strain rate as the loading strain rate under dynamic stress equilibrium. A C11000 half-hardened copper disk with a diameter of 6.35 mm and a thickness of 1.57 mm was selected as the front pulse-shaper while two C11000 annealed copper disks employed as the rear pulse-shapers were 2.39 mm in diameter and 0.51 mm in thickness. Using this technique, the dynamic stress-strain loop at a strain rate of 420 s^{-1} for a NiTi shape memory alloy was determined (Song and Chen 2004c). The steel Kolsky bar used for the experiments had a 12.70-mm diameter. The striker, incident, and transmission bars had a mass density of 8100 kg/m^3, a Young's

modulus of 200 GPa, an elastic wave speed of 4970 m/s, and lengths of 305 mm, 1829 mm, and 762 mm, respectively.

The shape memory alloy studied in these experiments is composed of nominal 55.8% nickel by weight and the balance is titanium. The NiTi shape memory alloy has a specified density of 6.5×10^3 kg/m^3, an austenite finish transition temperature A_f of 5-18˚C, and a melting point of 1310˚C. The cylindrical specimens had a dimension of 4.76-mm in diameter by 4.76-mm in length.

Figure 5.18 shows the incident, reflected, and transmitted pulses at the strain rate of 420 s^{-1} obtained with the modified Kolsky bar during both loading and unloading phases (Song and Chen 2004c). The fact that the difference between the incident and reflected pulses nearly overlap the transmitted pulse, as shown in Fig. 5.18, indicates that the specimen was in dynamic equilibrium over nearly the entire duration of the experiment. In addition, the strain-rate history, which is proportional to the reflected pulse in Fig. 5.18, indicates that not only the loading strain rate but also the unloading strain rate was maintained at the same constant value (420 s^{-1}) for most of the experiment duration. The strain-rate signal flipped its sign from compression (loading) to tension (unloading) at the peak of the loading.

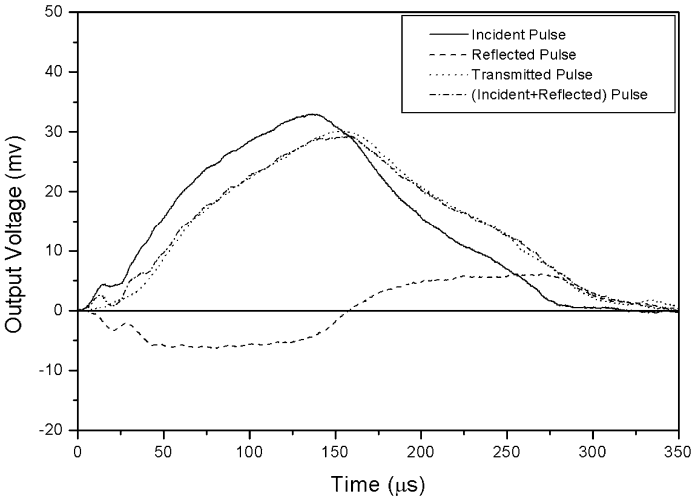

Figure 5.18 Experimental records of the bar signals on the shape memory alloy
(Reproduced from Song and Chen (2004c) with permission)

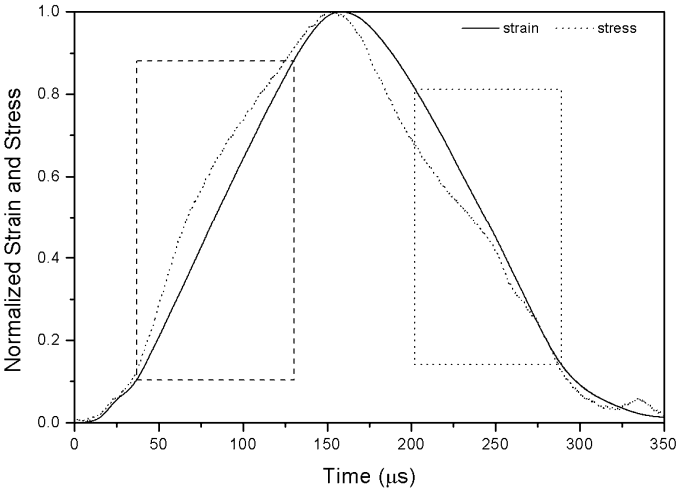

Figure 5.19 Stress and strain histories in the shape memory alloy specimen
(Reproduced from Song and Chen (2004c) with permission)

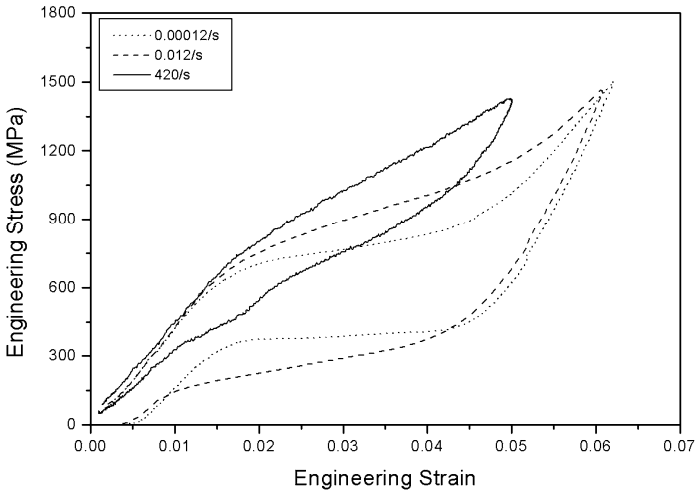

Figure 5.20 Compressive stress-strain loops of the shape memory alloy
(Reproduced from Song and Chen (2004c) with permission)

Figure 5.19 shows the detailed normalized strain and stress histories during the dynamic experiment (Song and Chen 2004c). The strain history is found to slightly lag behind the corresponding stress history. The dashed frames in Fig. 5.19 indicate the time ranges when the strain rate was maintained at the same value during loading and unloading.

Since the stress equilibrium in the specimen was also achieved within these time ranges (as shown in Fig. 5.18), the dynamic stress-strain loop at the strain rate of 420 s^{-1}, shown in Fig. 5.20, is an accurate measurement of the specimen response within the engineering strain ranges of 0.5% to 4.6% during loading and 0.7% to 4.3% during unloading (Song and Chen 2004c).

Due to the precise control of both loading and unloading histories, the stress-strain loops obtained from such dynamic experiments are directly comparable to those obtained under feed-back controlled quasi-static experiments. For the purpose of comparison, two quasi-static stress-strain loops of the NiTi shape memory alloy at the strain rates of 1.2×10^{-4} s^{-1} and 1.2×10^{-2} s^{-1} obtained with a hydraulically driven materials test system are also presented in Fig. 5.20. Both dynamic and quasi-static stress-strain curves exhibit some of fundamental characteristics of shape memory alloy behavior: an initial elastic behavior followed by a nonlinear superelastic behavior in the loading portion, and a nonlinear unloading behavior that had lower stresses at certain strains but a profile similar to that of the loading behavior. The loops show that the stress-strain behavior of the material is rate sensitive.

5.3.3 Alumina Filled Epoxy

Alumina filled epoxy is a composite material with alumina as fillers and epoxy as resin. Unlike most composite materials, the shape of the compressive stress-strain curve resembles that of a ductile metal. The composite has 43% by volume of alumina particles. The specimens were machined into cylinders with 12.7 mm in diameter and 6.35 mm in thickness from a large cylindrical billet of the alumina-filled epoxy composite. The Kolsky-bar setup is made of 7075-T651 aluminum alloy, with a common diameter of 19.05 mm, associated with a small annealed copper C11000 disk as the pulse shaper.

Figure 5.21 shows typical incident, reflected, and transmitted signals obtained from dynamic experiments at two different strain rates, 3.3×10^{2} s^{-1} and 7.3×10^{2} s^{-1} (Song et al. 2009c). The use of the pulse

shaper produces an extended rise time in the incident pulse, giving the specimen sufficient time to achieve dynamic stress equilibrium, which can be evaluated with (3.4). The equilibrium was examined in each experiment conducted. Figure 5.22 shows that the specimen reaches stress equilibration ~50 microseconds after initial loading (Song et al. 2009c). In addition, the shaped incident pulse minimized wave dispersion. Varying the dimensions of the copper pulse shaper and striking speed generates incident pulses with similar profiles but different amplitudes to achieve different constant strain rates in the specimen.

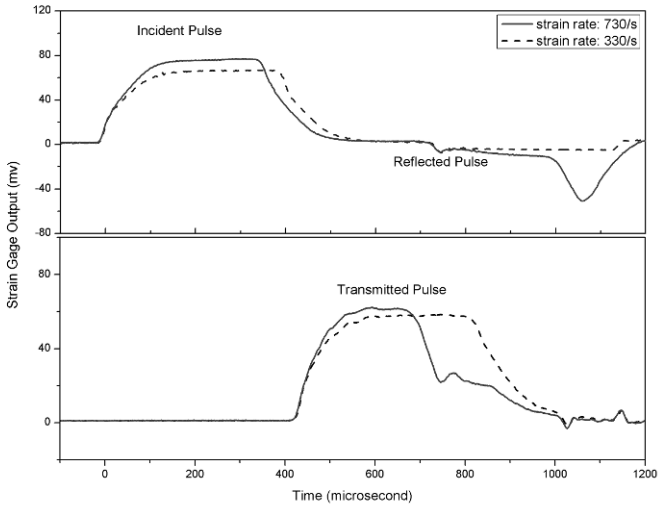

Figure 5.21 Experimental records from Kolsky-bar experiments on alumina-filled epoxy composite
(Reproduced from Song et al. (2009c) with permission)

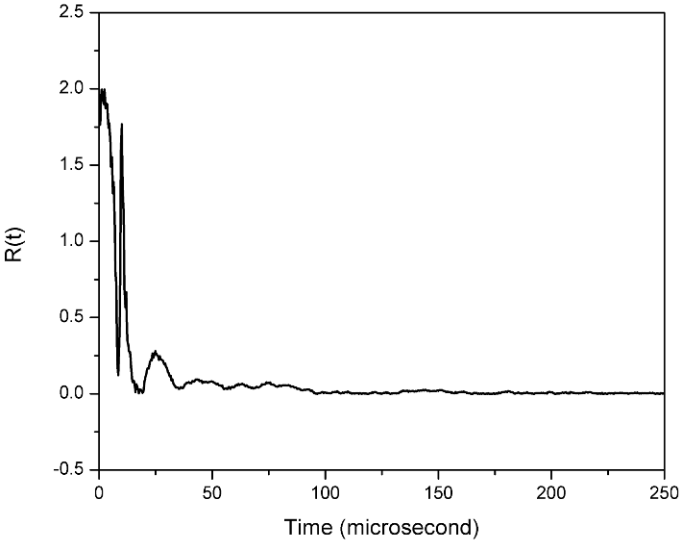

Figure 5.22 Dynamic equilibrium process in the specimen
(Reproduced from Song et al. (2009c) with permission)

The reflected pulse for the experiment at 330 s^{-1} in Fig. 5.21 has a long plateau, indicating the specimen is at a constant strain rate without catastrophic failure. By contrast, for the experiment at the strain rate of 730 s^{-1}, the reflected pulse has a higher plateau as expected but is followed by a sharp spike. This sharp spike corresponds to a sudden increase of strain rate due to material failure and loss of load-bearing capacity of the specimen. We have seen this type of signals in Chapter 3 dealing with brittle materials. The profiles of the transmitted pulses shown in Fig. 5.21, which are proportional to the stress histories in the specimens, indicate that the alumina-filled epoxy behaves similarly as an elastic-plastic material. The amplitude of the transmitted pulse is observed from Fig. 5.21 to increase with increasing strain rate, which indicates the strain-rate sensitivity of the material. Another detail worth being noticed is that the stress in the experiment at 330 s^{-1} drops because of unloading. Contrarily, the stress for the experiment at 730 s^{-1} decreases due to the failure of specimen.

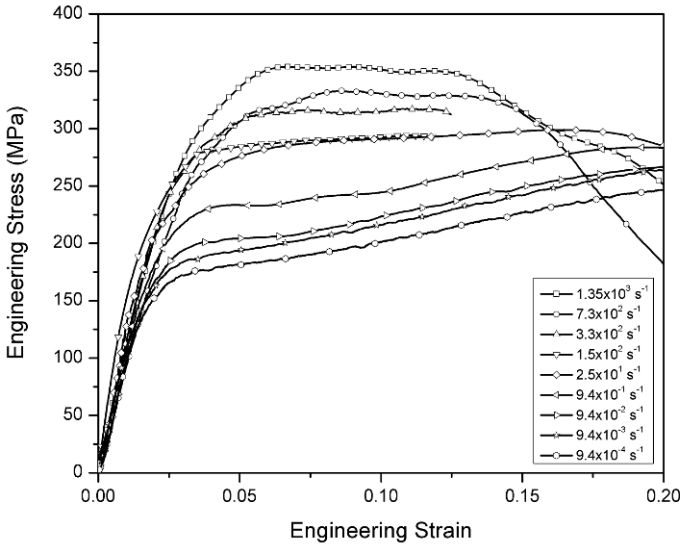

Figure 5.23 Compressive stress-strain curves of the alumina-filled epoxy composite
(Reproduced from Song et al. (2009c) with permission)

The stress-strain curves at various strain rates are shown in Fig. 5.23 (Song et al. 2009c). All stress-strain curves are very similar in their elastic behavior. The modulus of elasticity was measured approximately 12 GPa, which is not sensitive to strain rate within the range covered here. However, both yield strain and flow stress increase with increasing strain rate. In the quasi-static stress-strain curves obtained at the strain rates below 9.4×10^{-1} s^{-1}, an apparent work-hardening behavior is observed. However, when the strain rates are above 9.4×10^{-1} s^{-1}, the work-hardening behavior disappeared. The eventual failure strain decreases from approximately 20% at 9.4×10^{-4} s^{-1} to 12% at 1.35×10^{3} s^{-1}, although the macroscopic failure mode of the specimen was observed to be similar under both quasi-static and dynamic loading conditions.

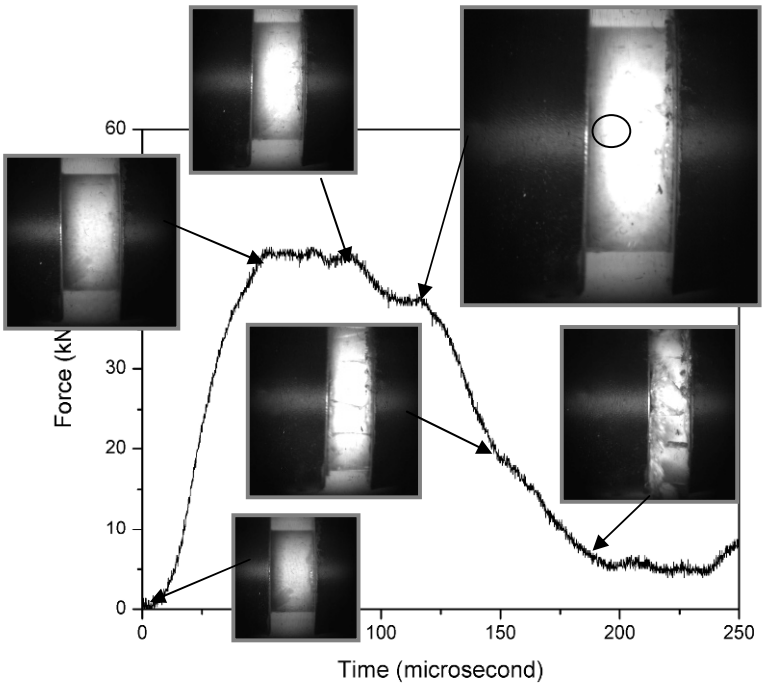

Figure 5.24 Dynamic damage and failure process in the specimen
(Reproduced from Song et al. (2009c) with permission)

Figure 5.24 shows a typical failure process and the corresponding force history in the specimen during a dynamic experiment at 1.35×10^3 s^{-1} (Song et al. 2009c). The images were taken with a Cordin 550 high-speed digital camera at a rate of 100,629 frames per second. As shown in Fig. 5.24, when the deformation of the specimen is clearly beyond the elastic range, say, near 100 μs on the time scale, no macroscopic cracks are visible on the specimen surface. When the loading is applied for 120 microseconds, the first surface crack is barely visible near the center of the specimen from the left end face. At this time, the force in the specimen has decreased from the peak. It is very likely that cracks have initiated earlier either inside or on the back surface of the specimen which could not be imaged. As the visible crack density increases on the imaged surface, the load-bearing capacity of the specimen

continues to decrease. Eventually, the specimen cylinder was split into several columns parallel to the loading direction.

5.3.4 Lead-free Solder

Solder joints in microelectronics devices are subjected to high-rate loading conditions in impact-related applications. For example, mobile electronics applications and automotive electronics devices subject the solder joints to impact and vibration, where the strain rates can be up to the order of 10^3 s^{-1}. Efficient design of the solder joints requires accurate material models that describe the high-rate behavior of the solder materials, which must be experimentally determined. In this group of Kolsky-bar experiments, the dynamic compressive behavior of a lead-free solder, Sn3.8Ag0.7Cu, was measured at various strain rates (Chan et al. 2009). The solder is relatively soft among the metallic materials family. Aluminum bars were used to facilitate enhanced transmitted wave signals. Copper tubes and disks were used as pulse shapers at strain rates of $220s^{-1}$ and $700s^{-1}$, respectively, to achieve constant strain rates under dynamic equilibrium.

Figure 5.25 shows a typical set of Kolsky-bar experimental records of the incident, reflected, and transmitted pulses. As shown in Fig. 5.25, the shaped incident pulse produces a reflected pulse with a flat plateau. This indicates a constant strain rate in the specimen if dynamic equilibrium is achieved, which is verified by the comparison of the force histories in front and on the back of the specimen, as shown in Fig. 5.26. The nearly overlapped force histories prove that the specimen is indeed loaded by equilibrated axial forces.

The validity of all Kolsky-bar experiments is checked. The data are then reduced to a group of compressive stress-strain curves as shown in Fig. 5.27. To investigate the strain-rate effects, quasi-static stress-strain curves are also shown in the figure. The results clearly demonstrate that the constitutive behavior of this lead-free solder is rate dependent, which must be accounted for in material model development.

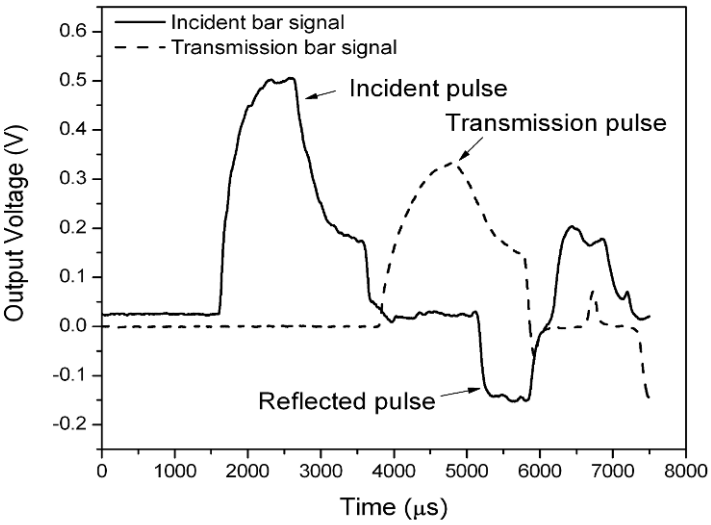

Figure 5.25 Experimental records from solder tests

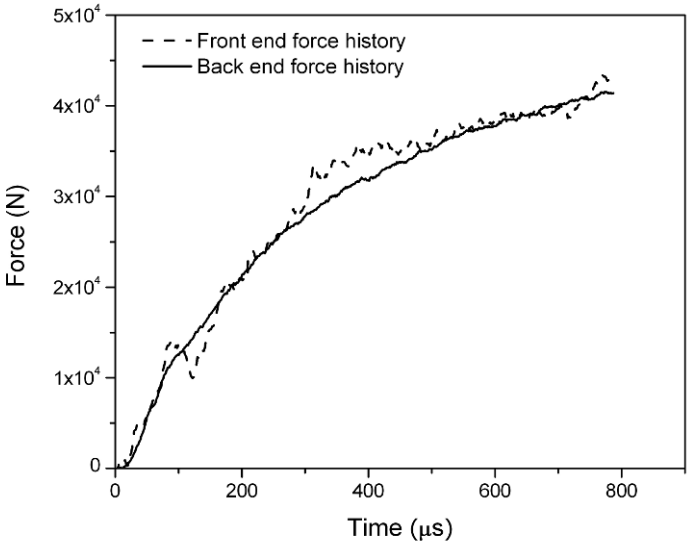

Figure 5.26 Dynamic equilibrium process in the solder specimen

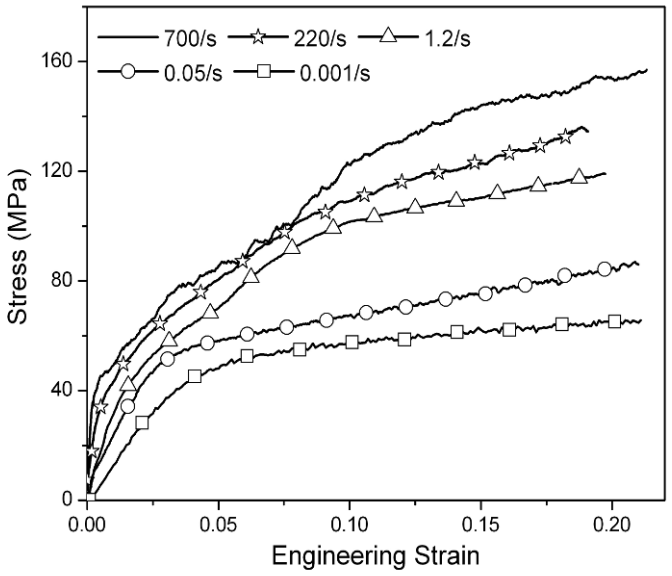

Figure 5.27 Compressive stress-strain curves of Sn3.8Ag0.7Cu solder